Europa's Radiation Environment and Its Effects on the Surface

C. Paranicas
Johns Hopkins University Applied Physics Laboratory

J. F. Cooper
NASA Goddard Space Flight Center

H. B. Garrett
NASA Jet Propulsion Laboratory/California Institute of Technology

R. E. Johnson
University of Virginia

S. J. Sturner
NASA Goddard Space Flight Center and
University of Maryland Baltimore County

Europa's orbit in the radiation environment of Jupiter is reviewed as is the influence of the neutral gas torus on the surface weathering of that moon. Data and fits to charged particle intensities in the 1-keV to the tens-of-MeV energy range are provided near Europa. Leading/trailing hemisphere differences are highlighted. Effects of charged particles on the surface of Europa, such as sputtering and chemistry, are reviewed.

1. INTRODUCTION

Charged particles trapped in Jupiter's rotating magnetosphere continuously overtake Europa in its orbit. At sufficiently high energies, these particles are relatively unaffected by the tenuous atmosphere of the satellite and instead bore directly into the ice before losing much energy. For example, energetic electrons and their bremsstrahlung photon products can directly affect the top meter of the icy regolith, which is also processed by meteoritic impact gardening (*Cooper et al.,* 2001; *Chyba and Phillips,* 2001). Charged particle irradiation of ice produces a number of new species as described in the chapter by Carlson et al. Those that are volatile at the ambient temperature, such as O_2, populate the atmosphere, whereas those that are more refractory, such as H_2O_2, can be detected as trace species in the ice. In addition to the chemical weathering of Europa's surface, the bombarding energetic particle flux drives species into the gas phase, a process called "sputtering." This produces a thin atmosphere above Europa's surface as described in the chapters by Johnson et al. and McGrath et al. Extrapolation from laboratory data to the quantification of radiation effects on Europa's surface and atmospheric environment requires modeling of the longitudinal and latitudinal distributions of energy deposited per unit volume vs. depth into the surface. It is also useful to characterize ranges of temporal variation caused by jovian magnetospheric activity and other effects. Therefore a central goal of this chapter is to provide estimates of the average energy vs. depth distributions at representative locations on the surface and to describe variations one might expect. We will also estimate the principal effects produced for different radiation types.

In section 2 of this chapter, we will discuss the jovian radiation environment to provide a context for Europa. In particular, we note the relative levels of radiation among the inner satellites as potentially important for differences in surface weathering. We also point out that Europa's orbit coexists with a cold neutral gas torus. This gas influences all ions up to the few-MeV range because of charge-exchange collisions that create energetic neutral atoms (ENAs) with energies reflective of their parent ion. In section 3, we turn our attention to the environment close to the satellite itself. We provide recent fits to the electron and ion data that describe the intensity of these trapped particles near Europa's orbit. We cover the energy range from about 1 keV to tens of MeV. We will also elaborate on the asymmetric bombardment of Europa by electrons, which has consequences for surface processing.

In section 4 of this chapter, we describe some of the effects of the radiation environment on the surface itself. A good recent summary of the consequences of charged particle weathering of Europa's surface can be found in *Johnson et al.* (2004) and references therein. *Cooper et al.* (2001) provide a table (their Table II) of surface irradiation parameters for the icy satellites. It is not our intention to repeat that material here but to mention highlights and updates since some of the earlier publications. In particular, we will extend some of our previous ideas on the nonuniformity of the surface bombardment. A central reason for improved modeling of space weathering effects on exposed surfaces in space is to determine the chemical compo-

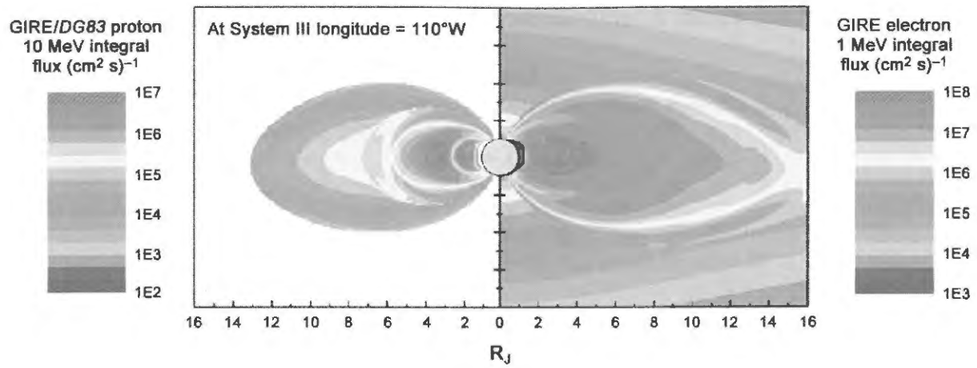

Fig. 1. See Plate 26. Contour plots of the GIRE/*DG83* model E > 10 MeV integral proton (left) and E > 1 MeV electron (right) fluxes for the vovian magnetosphere radiation region. The model provides the flux as a function of position, energy, and pitch angle. The fluxes presented here have been integrated over pitch angle. Note that outside the contour of L = 12, the proton model is set to 0, whereas the electron model fluxes outside L = 16 are only approximate since they are not considered trapped in the model (see *DG83* for details). Figure courtesy of I. Jun.

sition of materials intrinsic to Europa as compared to those originating from the external influence of magnetospheric particle irradiation. For example, the observed concentration (*McCord et al.*, 1998, 1999) of hydrated sulfate materials on the trailing hemisphere, recently confirmed by New Horizons observations (*Grundy et al.*, 2007), is strongly suggestive of connections to the corotating magnetospheric plasma, including iogenic sulfur ions (*Carlson et al.*, 1999, 2002, 2005; *Paranicas et al.*, 2001), but this connection is less clear at smaller scales of surface lineaments (*Geissler et al.*, 1998; *McCord et al.*, 1998) (see also the chapter by Carlson et al.). Galileo Solid State Imaging (SSI) and Near-Infrared Mapping Spectrometer (NIMS) multispectral data indicate compositional differences are present between specific surface features with respect to the surrounding terrain (*Carlson et al.*, 2005). It has also been observed that these features appear to brighten with age (*Geissler et al.*, 1998). This brightening may be the result of long-term exposure to Europa's radiation environment (e.g., *Geissler et al.*, 1998; *Johnson et al.*, 2004). Alternatively, the sulfur may be endogenic (*McCord et al.*, 1998; 1999), for instance, as in salts that have been moved through the ice crust from the subsurface ocean of Europa, but then the hemispheric asymmetry remains to be explained. Comparisons of composition and brightness distributions in highly and minimally irradiated regions is an example of how to potentially settle questions of endogenic vs. exogenic origin.

2. EUROPA IN THE CONTEXT OF JUPITER'S RADIATION ENVIRONMENT

The radiation belt modeling of *Divine and Garrett* (1983; hereafter *DG83*) combined *in situ* data from the Pioneer and Voyager spacecraft with groundbased data to describe the fluxes of energetic charged particles in Jupiter's inner magnetosphere. Their modeling put the peak radiation in >1-MeV electrons close to about L = 3, using a dipolar model of the magnetic field of the planet. In their fits to the various datasets, >10-MeV ion intensities also show a peak close to the planet but fall off rapidly with increasing radial distance. Near Europa's orbit, R ≈ 9.4 R_J (here R_J = 71,492 km), and keeping in mind the different lower-energy limits, the MeV ions are already substantially reduced from their peak, whereas the MeV electrons are somewhat lower than their peak but still significant. The *DG83* electron fluxes have been compared to Galileo orbiter measurements near Europa, Ganymede, and Callisto (*Cooper et al.*, 2001). The model and Energetic Particles Detector (EPD) fluxes in the 1-MeV range were found to agree well on the decrease in flux with increasing distance from Jupiter. At higher energies the electron data model of *Cooper et al.* (2001) was derived only from *DG83*. The *DG83* modeling for electrons has been superseded by the Galileo Interim Radiation Electron (GIRE) model (*Garrett et al.*, 2002, 2005). Model integral fluxes from GIRE/*DG83* are presented in Fig. 1.

The work of *Jun et al.* (2005) displayed Galileo EPD data, comparing the electron count rates and fluxes for energies ≥1.5, ≥2.0, and ≥11 MeV, for orbits over the whole mission. They found an approximately 2 order-of-magnitude increase in tens of MeV electrons from the orbit of Ganymede (R ~ 15 R_J) to that of Europa. *DG83*, its GIRE update, and *Jun et al.* (2005) also reflect a more or less steady-state structure in the energetic electron belt. This suggests that the population is persistent every time we sample it. Furthermore, from the work of *Jun et al.* (their Fig. 3), it is possible to estimate the variability of this population. Near Europa's orbital distance, the 1σ level of the ≥11-MeV electron flux is about a factor of 2–3 times the mean and the 2σ level is a factor of 10. These data include nearly all the Galileo orbits and are ordered in dipole L shell using the VIP4 model (*Connerney et al.*, 1998). (In a dipole field, the L shell can be calculated from $L = r/\cos^2\lambda$, where r is the distance from the center of the dipole and λ is the magnetic latitude of the point in question.) This spread is

probably an upper limit on the variability of that population since, for example, Jun and his colleagues did not separate the data by pitch angle.

Coexisting with the MeV particles, there is dense, cold plasma (see, for example, the chapter by Kivelson et al.) and medium-energy particles in the keV energy range. *Mauk et al.* (2004) have generated fit functions for the tens of keV to tens of MeV ion data obtained by Galileo. *Mauk et al.* (2004) present various moments of the distribution function by radial distance from Jupiter. In Fig. 2, we have used the fits from *Mauk et al.* (2004) to create plots of particle intensity by species and L shell at specific energies. Each panel shows a separate ion in the radial range from Io's orbit to about 20 R_J. The large gaps in coverage are due to the fact that Mauk et al. were only able to compute fits at specific locations in the magnetosphere. Typically we would expect such curves to rise inward toward the planet because as particles are transported inward they are energized and there are typically more charged particles at lower energies. It is notable in Fig. 2 that ions above about 500 keV continue to increase inward across Europa's orbit. On the other hand, lower-energy ions have dramatic changes at or near Europa's orbital distance.

The initial decrease (moving radially inward in L in Fig. 2) in the ion intensities below about 500 keV is likely caused by their loss to the neutral gas torus at Europa's orbit (*Lagg et al.*, 2003; chapter by Johnson et al.). Magnetospheric ions can undergo charge-exchange reactions with neutrals in the gas torus and leave the system as ENAs. Charge exchange cross-sections are large at low energies but begin to fall off rapidly for protons above about 100 keV and for O^+ above several hundred keV (e.g., *Lindsay and Stebbings*, 2005). If charge exchange is the dominant loss process for ions below about 500 keV near Europa's orbit, then these ions are not principally lost to the satellite's surface. It is likely then that the surface is not heavily weathered by these ions, as was believed prior to Galileo. This is not the case for MeV ions or electrons. Their mean intensities continue to rise radially inward to the planet, relatively unaffected by the gas.

One mechanism for populating such a neutral torus is collisions between corotating magnetospheric ions and neutrals in Europa's atmosphere. Neutral modeling by *Smyth and Marconi* (2006) shows high column densities of O and H_2 that peak in the radial dimension at Europa's orbit (see chapter by McGrath et al.). To further support the presence of neutral gas near Europa, *Mauk et al.* (2003) found evidence of ENA emissions from the region of the gas torus, with data from Cassini's Magnetospheric Imaging Instrument (MIMI) during that spacecraft's distant Jupiter flyby. Mauk and his colleagues correlated the ENA signal with the torus and not Europa itself (e.g., there are two emission peaks at the radial distance in question). To summarize our findings then, Europa is heavily weathered by MeV ions and electrons and by keV electrons with much higher intensities than at Ganymede or Callisto. The dominant mechanism of loss for medium energy ions near Europa's orbit is by charge-exchange collisions with neutrals in a gas torus.

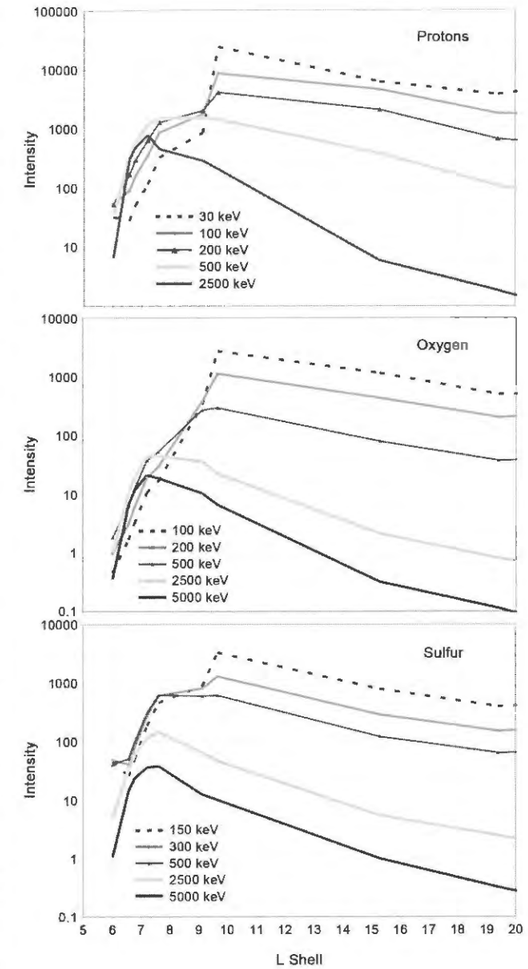

Fig. 2. Ion intensity (ions per cm² s sr keV) at constant energy. Values are computed at specific Galileo locations from fits to the full charged particle spectra reported by *Mauk et al.* (2004) and connected by lines for ease of viewing. The fit functions for all points used to create this graph are given in Table 1 of *Mauk et al.* (2004). In a dipole field, the L shell of Europa varies between about 9.3 and 9.7 R_J.

3. EUROPA'S RADIATION ENVIRONMENT

The various data analysis and modeling efforts mentioned above as well as other studies help to place the radiation environment of Europa in the context of the rest of the inner to middle magnetosphere. Europa's radius is ~1561 km and its mean orbital radius is ~9.39 R_J. Its orbit is tilted relative to Jupiter's equator (by about 0.466°) and is slightly eccentric (0.0094) (see *ssd.jpl.nasa.gov*). Because of the tilt of Jupiter's magnetic dipole, Europa makes excursions from the spin plane to approximately 10° north and

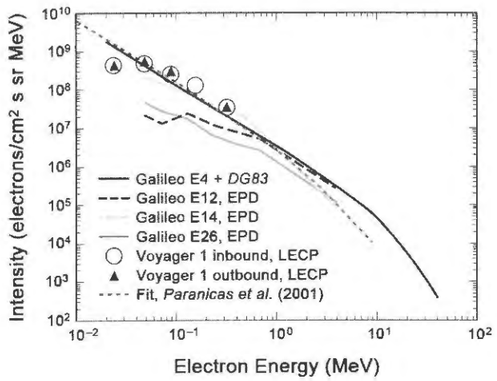

Fig. 3. Energy spectrum of electrons measured near Europa's orbit from various sources including *Cooper et al.* (2001) *Paranicas et al.* (2001) and the JPL model of *Divine and Garrett* (1983) as derived from Pioneer and Voyager data at Jupiter.

south magnetic latitude. The weathering of the moon depends somewhat on its magnetic latitude, since off the equator a fraction of charged particles do not have access to the moon's surface. However, this may be most important for weathering by the cold, heavy plasma. The relative position of Europa to the magnetic equator, which dictates the strength of the induced magnetic field (*Kivelson et al.*, 1999), will be a factor in particle access to the surface. In the following, we focus on the radiation environment at Europa's orbital distance and its variations. The data and fits we present are a compilation from different sources meant to he representative and are not a synthesis of all available jovian data to date.

In Fig. 3, we show a summary of the measured (and fit) electron intensity (electrons per cm² s sr MeV) from several sources near Europa or near its orbit. These include the *DG83* model, the Voyager 1 spacecraft Low Energy Charged Particle (LECP) detector data, and Galileo EPD data. Since the *DG83* model is based on Pioneer and Voyager spacecraft data, this set samples the main three generations of spacecraft that crossed Europa's orbit. The plotted fit to the intensity is

$$j(\text{counts per cm}^2\text{ s sr MeV}) = 4.23 \times 10^6\, E(\text{MeV})^{-1.58}\left(1 + \frac{E(\text{MeV})}{3.11}\right)^{-1.86} \quad (1)$$

One of the Galileo detectors was severely overdriven in the inner magnetosphere. For several of the data points plotted here, a correction was applied to recover, where possible, the actual rate. The high uncertainty in the rate near the lower energy end of the range probably explains the large variation and it should not be interpreted as variation in the local environment. For this figure, the omnidirectional flux of *DG83* was divided by 4π to obtain intensity per steradian for comparison.

Turning next to energetic ions near Europa, we compare data taken from several different Galileo encounters with Europa. In Fig. 4, we show energy spectra from the dominant ions separately: protons, oxygen, and sulfur. Fits to some of these ion data have been performed using the following function (*Mauk et al.*, 1994)

$$j(\text{counts per cm}^2\text{ s sr keV}) = C \times E(\text{keV})\frac{[E_1 + kT(1+\gamma_1)]^{-1-\gamma_1}}{1 + \left(E_1/e_t\right)^{\gamma_2}} \quad (2)$$

Galileo closest approach distances for these passes are approximately 692 km (E4), 586 km (E6), 201 km (E12), 1439 km (E19), and 351 km (E26) (data from JPL press release, 2003). *Kivelson et al.* (1999) provide details of these Europa passes and *Paranicas et al.* (2000) present energetic

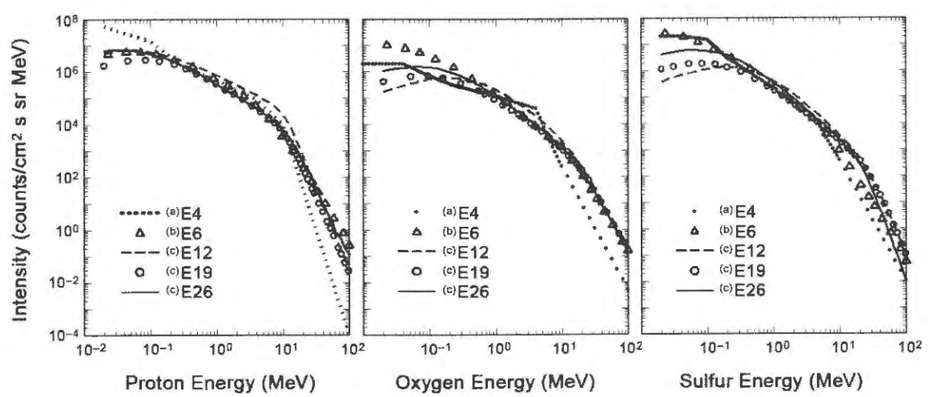

Fig. 4. Energy spectra by ion species computed from Galileo data during various near encounters of the satellite Europa. Sources of data include **(a)** *Cooper et al.* (2001), **(b)** *Mauk et al.* (2004), and **(c)** *Paranicas et al.* (2002).

TABLE 1. Fits to the individual ion energy spectra (by species) detected near Europa from *Mauk et al.* (2004) (to be used with equation (2)).

	H	He	O	S
C	2.79e + 06	8.02e + 04	9.19e + 06	1.42e + 07
kT (keV)	4.5	4.5	8.6	8.6
γ_1	1.213	1.213	1.647	1.599
e_t (keV)	6880	6880	10,838	5700
γ_2	4.177	4.177	2.793	2.616

charged particle data taken during them. For the Galileo E4 encounter, the fit parameters corresponding to equation (2) for various ions are given in Table 1.

On balance, there is a reasonably stable spectral shape with some variable range in absolute fluxes near Europa's orbit. By comparison, the inner magnetosphere of Saturn is injection dominated and some ions are not stably trapped. *Kivelson et al.* (1999) give Europa's position relative to the center of the current sheet during many of the Galileo flybys. They show that during E12, Europa was close to Jupiter's magnetic equator, E19 is off the equator, and E4 and E6 (and E26) are increasingly farther off. In Fig. 4, the ion measurements made near the center of the sheet have some of the highest intensities at high energy, but there is no such trend at lower energy. It is important to keep in mind that several issues are involved in the observed level of variation including the presence of the neutral gas, activity levels in the system (e.g., injections), how the pitch angles are sampled, and instrument aging issues. Furthermore, for the nine Galileo/Europa encounters listed in *Kivelson et al.* (1999), the local time range is confined to 0948 to 1642. A more robust indicator of time variability is provided in the work of *Mauk et al.* (2004). They have calculated an integrated quantity (called the detector current) representing the fluxes of medium energy to few MeV ions over the whole Galileo mission. They find that near Europa there is about a factor of ~2 variation in this integrated quantity in the 4-yr period that is covered (with very sparse sampling). They suggest that a main variation in the detector current is the variations in the neutral gas density.

To complete the description of the energy range of interest to us here, we show model fluxes down to 1 keV in Fig. 5. These are computed near Europa's orbit, but no shielding by Europa that would attenuate the flux is included. Since the range between about 10 keV and 100 keV has been poorly sampled in the past, fluxes are computed as follows. Energetic particle fluxes are derived from the Divine and Garrett model. A cold Maxwellian component is fit at the lower energies. Then a κ distribution is used to join the 1-keV model fit to the more energetic fits. Because there are many more of these particles, particularly electrons, than in the more energetic tail of the distribution function, they are important for processing the surface. The range in water of a 10-keV electron is about 1.6 μm and the range of a 1-MeV electron is 4.2 mm (*Zombeck*, 1982). The range in water of a 10-keV proton is about 0.3 μm and of a 1-MeV proton is about 24 μm (NIST website, *physics.nist.gov/PhysRefData/Star/Text/contents.html*). Therefore the vast majority of ions in the particle distribution functions, i.e., those up to about 10 keV in energy, directly affect only that part of the surface at depths less than about 0.3 μm.

3.1. Injections

To further study the role of variability in Europa's space environment, it is useful to consider transient phenomena. *Mauk et al.* (1999) surveyed over 100 instances of ion and electron injections in Jupiter's magnetosphere. They reported that these injections are most frequently observed between about Europa's orbital distance and 27 R_J and occur at all System III longitudes and local times. Injections of the type Mauk et al. have catalogued, whether they are interchange or another physical process, likely energize ions and electrons as they transport them inward radially, conserving their first adiabatic invariant of motion (see *Walt*, 1994, for a definition and discussion). Injected particles then corotate with the magnetosphere and become dispersed over time. Because injections are localized features, it is expected that they will introduce a level of variability to the background flux, but are not expected to dominate it. In Saturn's inner magnetosphere, by contrast, injections can often be the dominant population because some ambient flux levels are so low. Finally, at Jupiter, injections as described above are certainly a source of the inner, trapped population but it is not well known whether they are the dominant or a secondary source. Other processes such as energization in place by non-adiabatic processes and radial microdiffusion also play a role.

3.2. Bombarding Particles

In this subsection, we turn our attention to how the charged particles actually bombard the moon's surface. Here it is important to review some basics of the particle motion because it is central to what we describe below.

The energy spectrum of all charged particles trapped in Jupiter's magnetosphere is often divided into a plasma range and an energetic charged particle range. This separation is guided, to some extent, by the fact that the cold plasma can be studied with a magnetohydrodynamic (MHD) approximation (e.g., *Kabin et al.*, 1999) in which plasma flows like a fluid onto and around the object. At keV energies and above, the individual particle motions become significant and a single-particle approach is more appropriate. This is partly true because the gyroradius increases with energy and the more energetic particles become sensitive to spatial gradients of the magnetic field and to the curvature of the local field lines. These effects lead to gradient-curvature drifts in planetary longitude as discussed below. Moments of the particle distribution function, such as total mass and total charge, are dominated by the plasma. So, for example, the requirement of quasi-neutrality is typically enforced at plasma energies. Other moments, such as energy flux and

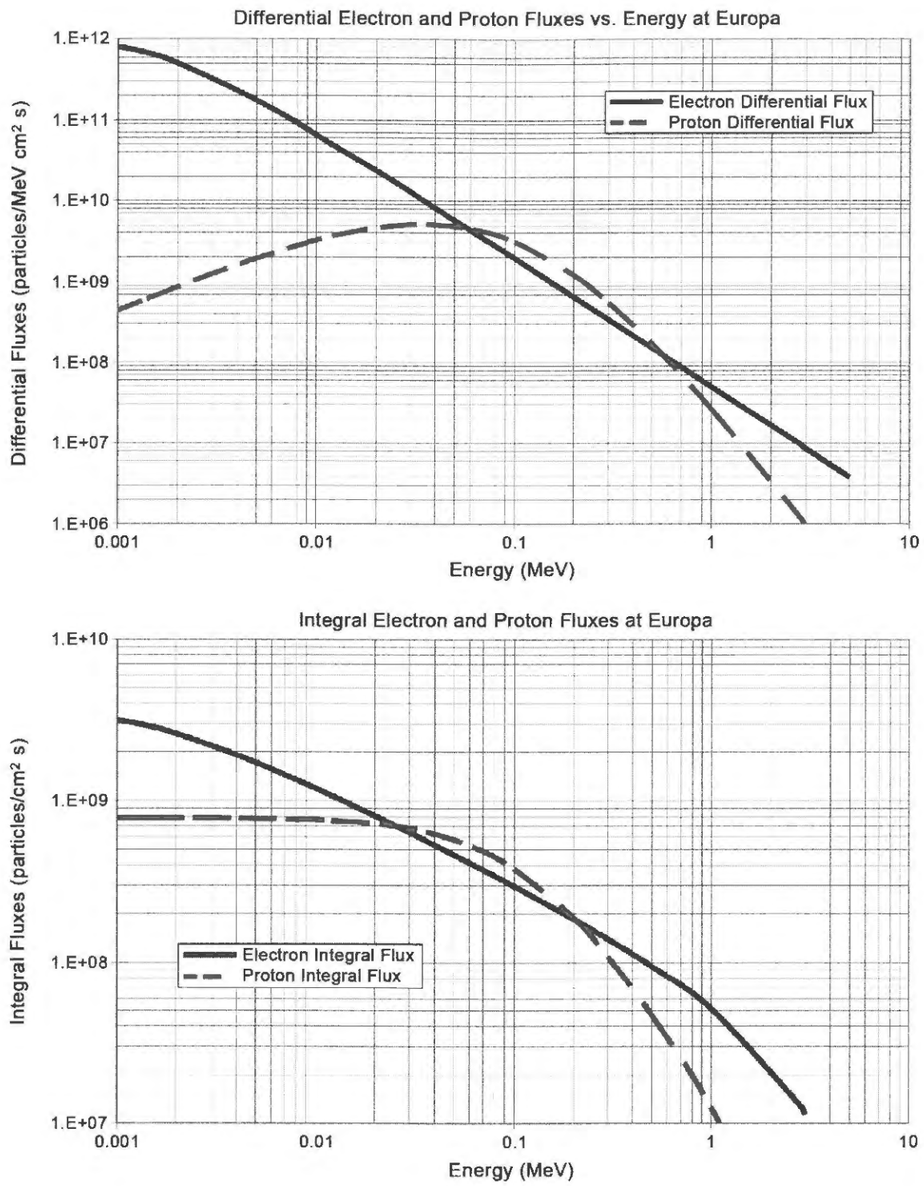

Fig. 5. Electron and proton fluxes computed from the DG radiation and warm plasma models. These correspond to a radial distance of 9.5 R_J.

particle pressure, can have important contributions from both parts of the particle distribution. Since we are interested in energetic charged particles here, we look at these particles from the perspective of individual particle motion.

Charged particles have three principle motions in the inner jovian magnetosphere: the gyration about the magnetic field line, the bounce along the field line between north and south mirror points — where the field becomes strong enough to reflect the particle — and the longitudinal motion. This third motion itself has two contributions: the so-called **E** × **B** drift and the gradient-curvature drift. The first drift dominates for charged particles at plasma energies and corresponds to the plasma flow speed. The **E** × **B** drift is due to the background magnetic field and an outwardly

pointing electric field (see *Khurana and Kivelson*, 1993, for a description of the origin of this field). Also, a complete description of charged particle motion in magnetospheres can be found in *Walt* (1994). For a rigidly rotating jovian magnetosphere, the plasma flow speed near Europa's orbit is approximately 118 km/s. Typically detected values are lower; for example, *Paterson et al.* (1999) report a speed that is about 80% of rigid corotation.

For the energies of interest to us here, it is also important to consider the gradient-curvature drift, which is caused by the deviations from a uniform magnetic field. In the corotating frame of the plasma, all ions drift in the same direction as the plasma flow and electrons drift in the opposite direction. This means that in the inertial frame, all ions are traveling slightly faster than the plasma corotation speed and all electrons slower. Above about 25 MeV, the gradient-curvature drift of electrons is comparable to the **E** × **B** drift in magnitude but opposite in direction and the electrons consequently have a net azimuthal motion that is retrograde, opposite to the prograde motion of Europa and the plasma flow. All the charged particles, except >25-MeV electrons, would therefore bombard Europa from the trailing hemisphere to the leading hemisphere. Here, by trailing hemisphere we mean the hemisphere that trails Europa in its motion around Jupiter. By convention, the center of the trailing hemisphere is 270°W longitude, where 90°W is the center of the leading hemisphere and 0°W points toward Jupiter.

Some equations that quantify these effects further are provided next. The net azimuthal speed of the charged particle's guiding center with respect to Europa can be expressed as

$$\omega = \Omega_J + \omega_D(L,E,\lambda_m) - \omega_k \tag{3}$$

Here Ω_J corresponds to Jupiter's rotation rate in rad/s, ω_k is the angular speed of Europa in inertial space, E is the kinetic energy in MeV, λ_m is the particle's mirror latitude, and ω_D is the gradient-curvature drift rate. Following *Thomsen and Van Allen* (1980) this drift rate can be written

$$\omega_D = \pm 6.856 \times 10^{-7} LE \frac{E + 2mc^2}{E + mc^2} \frac{F}{G} \tag{4}$$

We have modified the leading constant for Jupiter by taking the equatorial field strength as 4.28 G; L is L shell, mc^2 is the ion or electron rest mass in MeV, and ω_D is negative for electrons. We have preserved the *Thomsen and Van Allen* (1980) notation in using a function, "F/G", to express the dependence on the particle's mirror latitude (λ_m)

$$\frac{F}{G} = [1.04675 + 0.45333\sin^2\lambda_m - 0.04675\exp(-6.34568\sin^2\lambda_m)]^{-1} \tag{5}$$

The net azimuthal speed of the particle's guiding center, ω, is very important for understanding the bombardment of Europa. This speed can be compared with the speed of the particle along the magnetic field line to understand the satellite bombardment. For these purposes, it is useful to define a field line contact time, t_c, as

$$t_c = \frac{2 * \sqrt{R_E^2 - d^2}}{v} \qquad d \le R_E$$
$$t_c = 0 \qquad d > R_E \tag{6}$$

Here d is the impact parameter of the guiding center field line to Europa's center of mass and v is the net azimuthal speed of the guiding center field line with respect to Europa in kilometers per second. For charged particles of both species with energies less than about 200 keV, the maximum contact time in a rigidly corotating magnetosphere is about 30 s. This can be compared with the particle's half-bounce time, the time it takes a charged particle to travel from the magnetic equator to its magnetic mirror point and back to the equator. For a 100-keV charged particle with an equatorial pitch angle of 45°, the half-bounce time is about 7 s for an electron and 271 s for a proton (see Table 2). Therefore, for 100-keV protons, the contact time is much shorter than the half-bounce time. This means not all bounce phases have yet come into contact with Europa. Therefore, 100-keV and lower-energy protons are at least in principle capable of bombarding all points on Europa's surface with approximately the same flux.

Pospieszalska and Johnson (1989) presented a detailed analysis of ion bombardment of Europa including gyroradius effects. For a charged particle with an equatorial pitch angle of 45° and a kinetic energy of 100 keV, the ratio of the particle's gyroradius to the moon's radius is 0.001 (electrons) and 0.041 (protons). For electrons, a guiding center approximation is usually sufficient, but for ions it is often important to include the gyroradius explicitly. *Pospieszalska and Johnson* (1989) found that for 1-keV sulfur ions, the bombardment pattern on Europa's surface heavily favored the trailing hemisphere, with some of these ions reaching the leading hemisphere. At higher energies, e.g., for 30-keV and 140-keV sulfur ions, there is some leading-trail-

TABLE 2. Charged particle parameters near Europa; all equatorial pitch angles are 45° and mirror latitudes are 23.13°.

	E (MeV)	$t_b/2$(s)	r_g (km)	t_c (d=0, s)
Electrons	0.1	7.22	1.5	30.1
Electrons	1.0	4.2	6.5	31.51
Protons	0.1	271	62	29.69
Protons	1.0	86	197	27.82
O^+	0.1	1085	250	29.69
O^+	1.0	343	789	27.82
S^+	0.1	1535	353	29.69
S^+	1.0	485	1116	27.82

Formulas are based on the work of *Thomsen and Van Allen* (1980). For the calculation of the contact time, we assume that the magnetosphere is rigidly corotating at Europa's orbit.

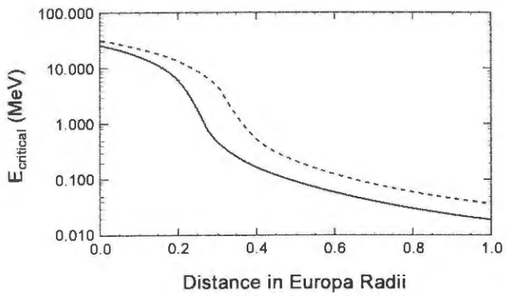

Fig. 6. Trapped electrons below the critical energy can bombard Europa's surface. The horizontal axis is the distance in the projected plane between the first point of contact of the electron's guiding center field line with Europa and the point of interest. The value 1.0 on the x-axis includes the pole. For this plot, electrons with an equatorial pitch angle of ~45° (solid line) and ~10° (dashed line) were used.

ing asymmetry in the bombardment pattern, but it was not a strong effect (see their Fig. 5). Updates to that work can be found in *Johnson et al.* (2004). Like 1-keV sulfur ions, energetic electron bombardment of Europa is expected to be very asymmetric. In the latter case, contact times are very large compared with the particle's half-bounce time. Electrons are therefore expected to bombard the moon close to the point of intersection between the moon and the guiding center field line (*Paranicas et al.*, 2007). For instance, for 5-MeV electrons of the same equatorial pitch angle, the contact time is about 38 s and the half-bounce time is about 4 s. Using the bounce and contact times, we show in Fig. 6 electron energies expected to be present in flux tubes attached to Europa. This critical energy is expressed as a function of distance in the direction of the plasma flow from the first point of contact of the field line with the moon. This distance is in Europa's equatorial plane. So, for example, on the central meridian of the trailing hemisphere, 270°W, at low Europa altitudes, there are very low fluxes of ~200-keV to 25-MeV electrons at north or south latitudes greater than 60°. This is the distance equivalent to 0.5 on the x-axis of Fig. 6 [i.e., cos λ = 1-distance (in R_E)]. Any electron flux present in this energy range would be from diffusive processes because the trapped electrons have already been lost in collisions with the moon's surface. By contrast, low-energy electrons (e.g., E < 20 keV) can strike the polar regions.

Using the energy cutoffs in Fig. 6, it is straightforward to compute the energy flux into Europa's surface. At any point on Europa's surface, (λ,φ), the energy flux can be calculated from

$$P(\lambda,\varphi) = \int j(E,\alpha,\xi)\, E\cos\psi(\alpha,\xi)\, \sin\alpha\, d\alpha\, d\xi\, dE \quad (7)$$

where $\psi(\alpha,\xi)$ is the angle at the surface point (λ,φ) between the vector antiparallel to the surface normal and the magnetic field vector at that point; α and ξ are the particle pitch and phase angles. In this general case, the integral at each point on the surface is taken over only those directions corresponding to flux pointing into the surface (see discussion in *Walt*, 1994), here values of ψ between 0° and 90°. In the usual approximation of gyrotropic and isotropic flux, the same integral is written down with a cos α replacing the cos ψ. The angular integral is then customarily expressed with the value π.

In Fig. 7, we plot P (λ, 270°W) calculated various ways for 80% of rigid plasma corotation. The distribution of energy into the surface depends on the fraction of rigid corotation of the plasma, the pitch angle distribution of the particles and their energy spectrum. In each case displayed in Fig. 7, the falloff of energy flux in latitude is fairly flat near Europa's equator, suggesting that the sensitivity to various approaches is not very important in that region.

In performing these calculations, we have assumed that Europa is an electromagnetically inert body and we do not consider factors such as its jovicentric magnetic latitude or the impact on total magnetic field of the moon's ionospheric currents or other electromagnetic contributions. The electromagnetic fields from Galileo have heen well described by a background field and an induced field of the satellite (*Kivelson et al.*, 1999). This induced field varies with Europa's position relative to the jovian plasma sheet, with the greatest induced field at the largest latitudes. The total field, background plus induced, at high moon excursion latitudes has magnetic field lines that do not go straight through the body hut are draped around it. (For a description of the full picture, see the chapter by Khurana et al.) This perturbation to the field is not dominant, so that a large deviation from the inert case is not expected. For example, the plasma flow close to the moon measured by the plasma instrument

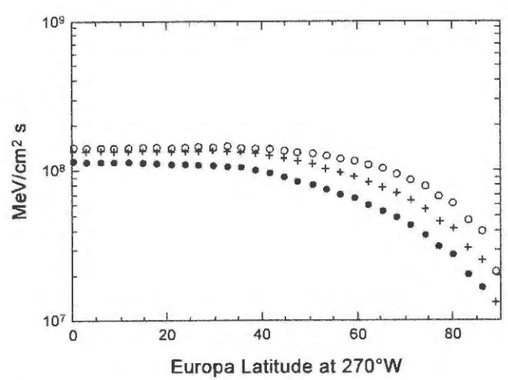

Fig. 7. Electron energy flux into surface as a function Europa latitude at 270°W. Plusses represent the integral using the energy spectrum in equation (1) and assuming an isotropic pitch angle distribution; the open circles use a simple power law, j = 1.0*E^{-2}, for comparison; and the filled circles use the energy spectrum above assuming the pitch angle distribution goes as sin α.

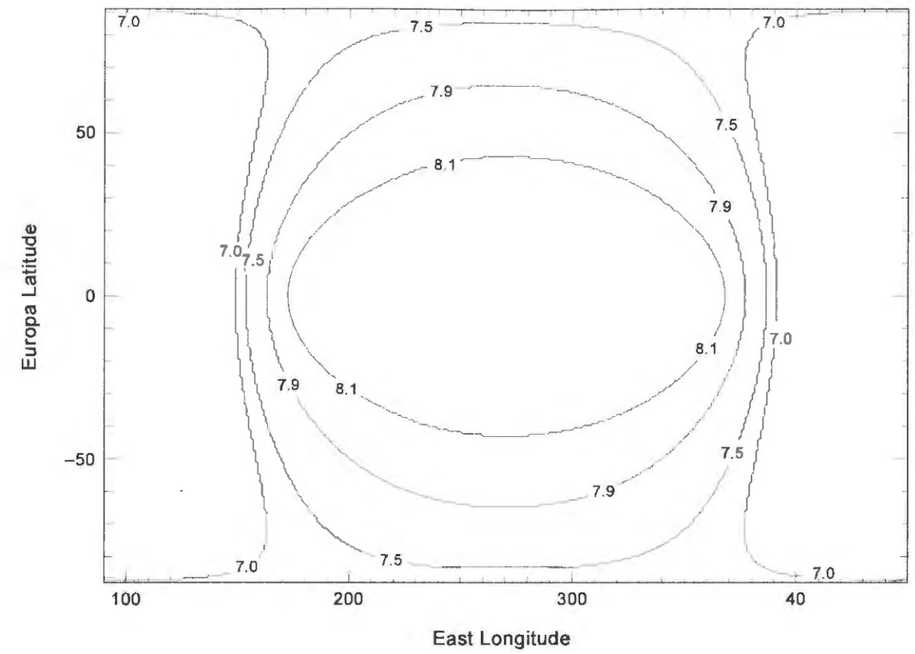

Fig. 8. Power per unit area into Europa surface for 10-keV to ~25-MeV electrons. Contours are labeled in units of log (MeV/cm² s). In this longitude system, the center of the trailing hemisphere of Europa is at 270°E.

on Galileo is not very distorted from the nominal corotation direction (*Paterson et al.*, 1999).

For completeness, we also present the value of P (equation (7)) as a function of Europa longitude and latitude. In Fig. 8, we show a contour plot of electron energy per unit area per second based on the energy spectrum given in equation (1). Here we assume the plasma flow is 80% of rigid and that Europa is an inert body whose orbit is in Jupiter's magnetic equatorial plane.

4. EXPECTED SURFACE EFFECTS

As previously reviewed hy *Johnson et al.* (2004), the magnetospheric particle population contributes to the surface composition of Europa in three major ways: (1) the low-energy magnetospheric plasma implants plasma ions, most notably iogenic sulfur, and contributes to sputtering; (2) more-energetic ions, the dominant sputtering agents, eject neutrals that contribute to an ambient atmosphere, cause transport of material across Europa's surface, and contribute to the neutral torus; and (3) energetic electrons and light ions, the primary source of ionization energy, drive the surface chemistry. Ignoring possible ionospheric diversion of the flow and effects of the then-unknown induced fields from the ocean, *Pospieszalska and Johnson* (1989) computed a bombardment pattern of 1-keV sulfur ions onto Europa's surface (their Fig. 5). In their calculation, the trailing hemisphere apex (i.e., 270°W, 0°N) received the highest flux and model fluxes fell away toward and onto the leading hemisphere. The implanted sulfur from radiation-induced chemistry and any endogenic sulfur will be in a radiation-induced equilibrium with a sulfate, SO_2, polymeric sulfur. Similarly endogenic or delivered carbon will be in radiation equilibrium with a carbonate, CO_2, and polymerized carbon. In addition, as discussed, the irradiation of the ice matrix will lead to H_2, O_2, and H_2O_2, all detected in either the atmosphere or the surface (see the chapter by Carlson et al. for a discussion of surface species and chemistry). An important goal of future work is to separately determine the role of these effects in producing the darkened terrain on the trailing hemisphere, the production of an atmosphere, and the population of the ambient plasma. In discussing the surface reflectance spectrum, we note that the various spectral signatures (UV, visible, IR) sample different depths. Therefore, implantation primarily affects the very near surface and electrons affect the material to greater depths. However, gardening huries the implanted sulfur, so that a separation by depth may not be straightforward. The similarity of the bombardment patterns of ~1-keV sulfur ions and energetic electrons (*Pospieszalska and Johnson*, 1989; *Paranicas et al.*, 2001) will only lend itself to separation if the sampling depth of the spectral signatures are

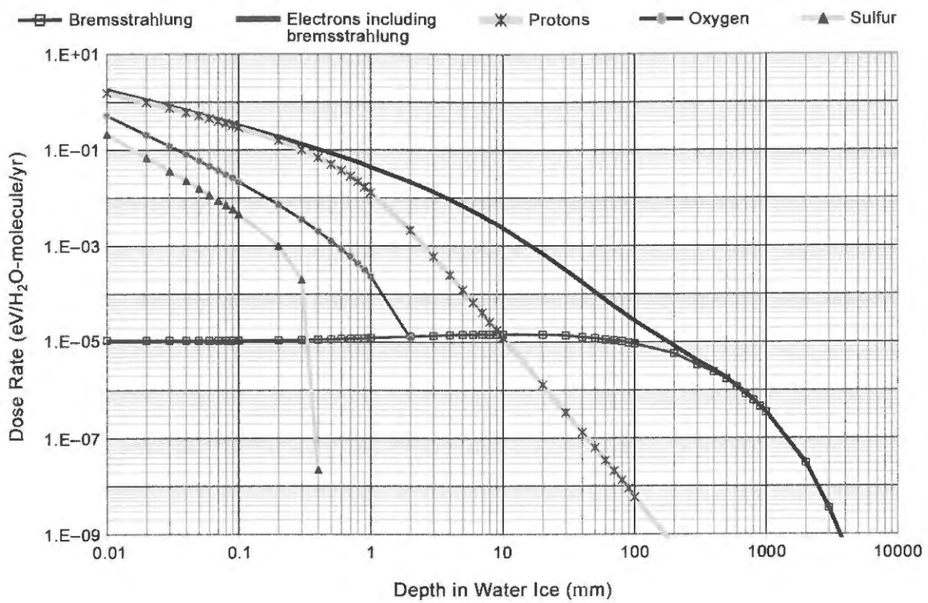

Fig. 9. Predicted dose rate vs. depth at the apex of Europa's trailing hemisphere by charged species using an input spectrum for various species and an ice surface. Heavy ions are stopped almost immediately in the water ice. At large depths, the electron dose rate becomes dominated by the contribution from secondaries (bremsstrahlung). This figure is based on the intensities of medium- to high-energy charged particles. See details in *Paranicas et al.* (2002).

carefully analyzed. Further understanding of the moon/plasma interaction (see the chapters by Kivelson et al. and Khurana et al.) will help us refine our understanding of the sulfur ion bombardment once the effects of the induced field are included. Such comparisons address a major theme of this chapter: the extent to which exogenic processes are understood in producing observable features on Europa.

As noted in the previous section, the penetration depth of charged particles into ice depends on a number of factors, including charged-particle type and energy. A published estimate of the maximum dose vs. depth for charged particles into water ice at Europa's surface is shown in Fig. 9. These curves were created using a Novice radiation transport code and various energy spectra based on spacecraft data as described in *Paranicas et al.* (2002). An important feature of this plot is that the trailing hemisphere dose near Europa's equator is dominated at almost all depths by the electrons. This fact, combined with the asymmetry of the electron dose onto Europa's surface described above, led us to compare the dose pattern with the distribution of hydrated sulfates, potentially sulfuric acid hydrates (see *Paranicas et al.*, 2001, and references therein). The favorable comparison suggested that the surface material in the dark regions, which are primarily on Europa's trailing hemisphere, are radiolytically processed to significant depths by the energetic electrons. This also suggests other leading/trailing asymmetries, such as that of 1-keV sulfur ions, might be a secondary effect.

Impacts of the various radiation dosage components in Fig. 9 must he considered separately for surface effects on the leading and trailing hemispheres. Energetic heavy ions deposit most of their energy very close to the surface. Noting that grain sizes are ~50 μm, sulfur ions are only implanted into the surficial grains and the heavy ions are the primary sputtering agents having the highest rate of energy loss per ion at submicrometer depths. Because of the dynamics of their motion, these heavy ions globally impact the surface in both hemispheres. Therefore, the curves in Fig. 9 for ions can be used as approximate dose-depth curves everywhere on the surface of Europa. The protons and especially energetic electrons lose energy in the ice more slowly and deposit this energy at much larger depths. Energetic electrons deliver the most total energy to the trailing hemisphere and electrons between about 100 keV and 25 MeV have much less impact on the leading bemisphere. Just above 25 MeV, electrons preferentially impact the leading hemisphere and become more uniform over the surface with increasing energy above that.

In Fig. 10, we show a dose-depth presentation with specific energy ranges represented separately. These are based on our implementation (*Sturner et al.*, 2003; *Cooper and Sturner*, 2006, 2007) of the GEANT transport code with

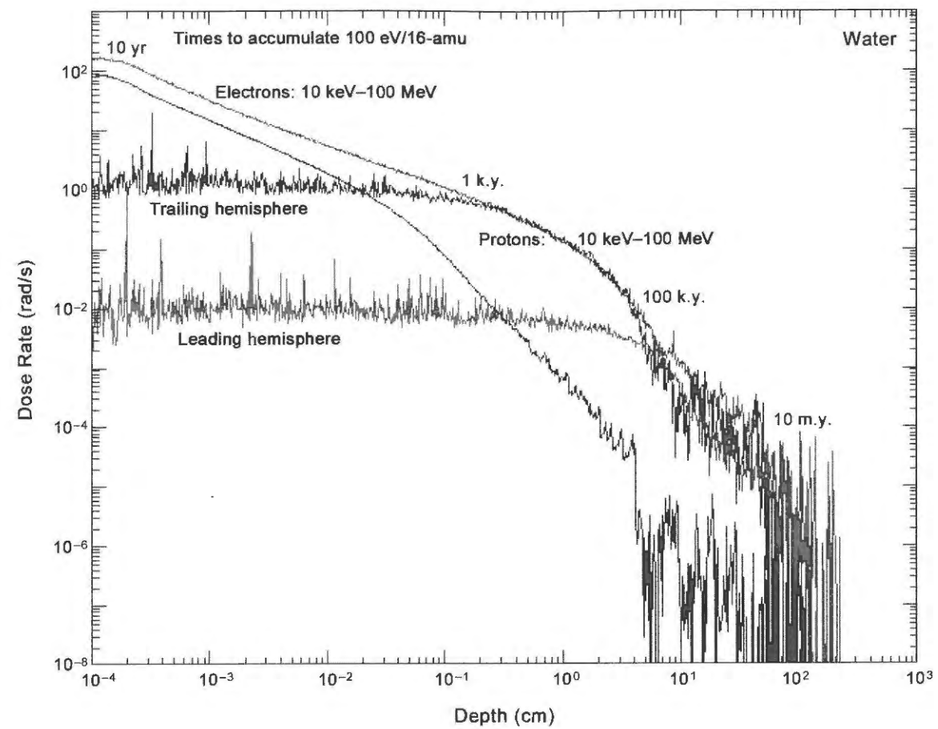

Fig. 10. After *Cooper and Sturner* (2006). Dose rate vs. depth where 1 rad/s is equal to 100 erg/gm/s or about 0.06 eV/H_2O-molecule/yr. The curve labeled "trailing hemisphere" includes the dose rate of 1–20-MeV electrons only, whereas the curve below it labeled leading hemisphere displays the dose rate of 20–40-MeV electrons that drift opposite to corotation. The uppermost of all the curves is the dose rate corresponding to electrons from 10 keV to 100 MeV and the dose rate from protons between 10 keV and 100 MeV follows this curve below it. Spikes and fluctations in the computed curves arise from statistics of limited number of Monte Carlo events used in the simulations and not from physical processes. Times in years are shown to give chemically significant (most bonds are broken at least once) dose of 100-eV/16-amu (60 Gigarads) at selected dose levels.

inclusion of all significant nuclear and electromagnetic (e.g., bremsstrahlung) interactions for primary and later generation particles and γ-ray photons. These researchers further employed the semi-analytical moon interaction model of *Fillius* (1988) to derive energy ranges of electrons primarily impacting the trailing (1–20 MeV) and leading (20–40 MeV) hemispheres of Europa with highest probability. Broadly speaking, the dosage profiles for these two respective energy ranges suggest a drop by 2 orders of magnitude from the trailing to the leading hemisphere for MeV electrons. However, at each surface point and at each depth, care must be taken in assessing which particles dominate the dose. For instance, around the apex of the leading hemisphere, the 10-keV to 100-MeV proton dose dominates over the 20–40-MeV electron dose down to about 3 mm from Fig. 10. Selected times to accumulate a net dose (from all sources) of ~100 eV per water molecule, equivalent to a volume dosage of 60 Gigarads per gram of H_2O, are also indicated. These times are only ~10 yr at the micrometer level but 10^6 yr at tens of centimeters. On multi-billion-year timescales the dosage effects of cosmic rays penetrating from outside the Jupiter magnetosphere for energy deposition to several meter depths in the surface ice, and decay of naturally abundant radioisotopes (e.g., K^{40}) throughout the ice crust to kilometers in depth (*Chyba and Hand*, 2001) become important.

4.1. Radiolysis

As described in the chapter by Carlson et al., the energy deposited by the charged particles and also by the UV photons cause dissociations and chemical reactions in Europa's surface. A principal product is hydrogen peroxide based on the reaction $2\,H_2O \rightarrow H_2O_2 + H_2$. Since H_2 is volatile and mobile in ice at the temperatures relevant to Europa's surface, it diffuses out more readily than other products. The

escaping H_2 is light and readily lost to space, as described in the chapter by McGrath et al. Therefore, the ice surface becomes oxygen rich, a principal result of the intense irradiation of the surface. In addition to H_2O_2, O_2 is produced and carbon and sulfur are present in oxidized forms: CO_2 and possibly H_2CO_3, SO_2, and hydrated sulfuric acid respectively (see the chapter by Carlson et al.).

When O_2 is created in the ice, it can diffuse out if it is near the uppermost layer, otherwise it can be trapped at depth (*Johnson and Jesser,* 1997; *Shi et al.,* 2007). Burial by meteoritic impact ejecta, which occurs faster than erosion by ion sputtering (*Cooper et al.,* 2001), can increase steady-state accumulation rates of trapped O_2 and other radiolytic product species. Detection of condensed high-density phase O_2 on the surface (e.g., *Spencer and Calvin,* 2002) indicates that such trapping is occurring in the ice matrix or perhaps, within more stable mixed gas clathrate structures (*Hand et al.,* 2006) in the surface ice of the trailing hemisphere. The O_2 that escapes on production or is caused to diffuse out by the incident plasma is the source of the tenuous oxygen atmosphere over Europa (see chapters by Johnson et al. and McGrath et al.). Under long-term irradiation a rough steady state is achieved with fresh products formed and trapped products destroyed. In this situation, the H_2 and O_2 arising from H_2O are naturally produced in about a 2:1 ratio. The size of the steady-state yield of H_2 and O_2 depends not only on the radiation dose but also on the ambient surface temperature.

Chemical production rates in surface regions with relatively pure water ice can be estimated from the electron energy fluxes and from G values: the number of a new chemical species produced (or destroyed) per 100 eV of deposited energy. As previously reviewed by *Johnson et al.* (2004), these values vary somewhat with radiation type and energy and the presence of trace species in the ice, with a rough average value of G ~ 0.1 for radiolytic yield of H_2O_2 (see chapter by Carlson et al.). Using this G, the average integrated column production rate of H_2O_2 in icy regions of Europa's surface is ~5×10^{10} $H_2O_2/cm^2/s$ (*Cooper et al.,* 2001). The regional rate would be lower on the leading hemisphere but there are significant contributions there from protons and heavier ions as discussed. Higher meteoritic impact rates on the leading hemisphere would give correspondingly higher radiolytic product burial rates and increase the net accumulation. However, in modeling the bound component of the atmosphere, ballistic transport and the fate of the sputtered species on redeposition have to be considered. For instance, *Cassidy et al.* (2007) have modeled atmospheric formation from surface irradiation and find that the darker sulfate regions of the trailing hemisphere may be net sinks, not sources, for O_2. Therefore, the long lifetime of O_2 and the possible dearth of reactive species can result in a comparable O_2 atmosphere on the less-irradiated leading hemisphere.

Oxygen chemistry provides a source of O_2 for the surface and atmospheric environment (*Johnson et al.,* 2003) with possible effects for the crustal chemistry and astrobiological potential of Europa. The surface-trapped O_2 might be conveyed by crustal processes to deeper levels, affecting the rheological properties of the ice crust (*Hand et al.,* 2006), and providing a significant oxidant source for the putative subsurface ocean of Europa (*Cooper et al.,* 2001; *Chyba and Phillips,* 2001; *Chyba and Hand,* 2001). Since oxidants in the irradiated surface environment could destroy organics brought to the surface, future missions to Europa should consider conditions of surface irradiation and oxidant concentration in the choice of surface sites for remote and landed measurements. Sites with relatively low irradiation, e.g., the leading hemisphere and topographically shielded spots in other locations (*Cooper and Sturner,* 2006), and low oxidant (O_2, H_2O_2) concentrations might be preferable in any searches for organic materials. On the other hand, concentrations of CO_2 in association with H_2O_2 might be indicative of ongoing radiolytic oxidation of near-surface organics either emerging from a subsurface repository or earlier deposited by an impact event.

4.2. Sputtering

In comparison to the volume ice effects of radiolysis dominated by electrons and protons, sputtering mainly applies to erosion of upper molecular layers by impact of highly ionizing particles, e.g., the heavy sulfur and oxygen ions originating from the Io torus that have undergone acceleration in the magnetosphere of Jupiter. Sputtering liberates molecules that transiently populate the atmosphere and redistribute surface material or escape Europa's gravity. Lighter molecules, such as H_2, may escape more easily, leaving behind an atmosphere that is richer in heavy molecules such as oxygen (see also the chapter by Johnson et al.). Sputtering primarily carries off water molecules from the icy surface, but also carries off any newly formed and intrinsic species trapped in the ice. For sufficiently high sputtering yields these trapped species could potentially include complex organics of high interest for astrobiology.

As discussed for H_2 above, a fraction of the surface ejecta escapes Europa's gravity; the neutral escape speed is about 2 km/s. The escaping neutrals produce an extended neutral atmosphere that is gravitationally bound to Jupiter (see chapter by Johnson et al.). Components of this nearly toroidal atmosphere (*Mauk et al.,* 2004; *Smyth and Marconi,* 2006) are ionized in a variety of ways. New ions are accelerated by the electromagnetic fields, i.e., they are picked up by the corotating magnetosphere. In this way, Europa's surface is a source of neutrals and ions to the local environment. It has been suggested that Europa is a net source of sputtered Na to the local magnetosphere (*Johnson,* 2000; *Leblanc et al.,* 2002; *Burger and Johnson,* 2004). This finding may extend to other endogenic species. Furthermore, at a much higher end of the ion energy range, *Cohen et al.* (2001) found that MeV carbon ions have a different radial intensity gradient in the magnetosphere than iogenic sulfur. This may originate in part from surface sputtering of Europa, Ganymede, and Callisto, but is complicated by known sources of carbon, such as the solar wind. The study of minor ion species at all energies can provide clues to origin, surface constituents, and energy and mass flow through magnetospheres.

The surface sputtering rate is determined by the energy spectra of ions and the yield, the number of neutrals ejected per incident ion. Furthermore, decomposition and loss of H_2 and O_2 from ice also puts surface material into the gas phase, so the net surface erosion rate has a temperature dependent component that dominates above ~100 K (chapter by Johnson et al.). *Johnson et al.* (2004) give a yield function that is a consolidation of many laboratory studies of the sputtering of water ice by the energetic plasma ions (updated at *www.people.virginia.edu/~rej*). Using their fit, the peak yield is $Y \sim 3.4*Z^{2.8}$, where Z is the nuclear charge of the ion. The peak yield occurs at an ion speed that can be expressed as $v^{max} = 2.72 \times 10^6 * Z^{0.334}$ m/s. This corresponds to a peak yield of ~3.4 for 39-keV protons, Y ~ 1149 for 2.5-MeV O^+, and Y ~ 8000 for 8.1-MeV S^+. Since the heavy ion yields peak in the low MeV, it has been assumed that, due to the falling energy spectrum of the charged particles, the total yield was dominated by the action of keV ions. The most recent estimate of the globally averaged sputtering yield from *in situ* data is ~2.4×10^{27} H_2O molecules/s (*Paranicas et al.,* 2002), ignoring the temperature dependent component and the contributions from ions below 1 keV/amu. Recent reevaluation of the sputtering data for the thermal plasma ions, for which both electronic and collision energy deposition apply, had important effects on the rates in the saturnian magnetosphere (e.g., *Johnson et al.,* 2008) but still indicate that the heavy ions are the dominant sputtering agents at Europa. This gives a globally averaged time of ~6.1×10^4 yr to erode 1 mm of ice (e.g., *Cooper et al.,* 2001). This estimate includes the three major ions of Fig. 4, but the sputtering yield is dominated by energetic sulfur ions. As noted previously from the same referenced work, the meteoritic impact burial time, ~10^3 yr per mm of ice, is shorter, so the Europa surface is buried by ejecta faster than it is eroded by sputtering.

As surface properties are better understood, sputtering rates will need to be refined. For example, microscopic structure and temperature can affect the sputtering yields. The porosity of Europa's regolith will reduce, by approximately a factor of 4, the effective sputtering yield of species such as H_2O that stick to neighboring grains with unit efficiency (*Johnson,* 1990, 1995, 1998; *Cassidy and Johnson,* 2005). Other species with low sticking efficiency, such as H_2 and O_2, more easily escape (see also the chapter by Johnson et al.), but some (O_2, CO_2, SO_2) can be trapped in inclusions (*Johnson and Jesser,* 1997; *Shi et al.,* 2007) or in mixed gas clathrates, wherever these are stable at the surface (*Hand et al.,* 2006).

Another surface property potentially affecting sputtering is surface charging, which can affect the access of low-energy species to the surface or the ejection of ions. Sunlit surfaces charge positively due to photoelectric emission of electrons, whereas other surfaces preferentially bombarded by magnetospheric electrons or protons can respectively accumulate negative or positive charge. Ejection of ions at the same charge as the surface would be enhanced by electrostatic repulsion and diminished for opposite signs. Neutral gas species undergoing electron attachment reactions, e.g., producing O_2^-, would have higher sticking efficiencies in sunlit regions. Maximal intensity electron bombardment of sulfate-rich regions in the trailing hemisphere may increase surface retention of such ions and thereby contribute to the observed non-ice chemistry. Accumulation and potential solid-state mobility of free charges in irradiated surface ices of Europa may also impact the electrical conductivity and electromagnetic properties of these ices with effects on moon-magnetospheric interaction modeling and on deep sounding of the interior with electromagnetic waves for ice radar and oceanic induced magnetic field investigations (*Gudipati et al.,* 2007).

4.3. Radiation Damage

Both penetrating and non-penetrating radiation produces defects in ice. In addition, water vapor is sputtered and redeposited, which can lead to an amorphous layer, depending on the surface temperature. Both processes occur at very low rates, so in principal can be annealed. Reflectance spectra suggest a thin amorphous layer, with crystalline ice forming at ~1 mm (*Hansen and McCord,* 2004). Based on Figs. 9 and 10, such a layer is likely formed by radiation damage produced by the energetic protons and electrons. In addition, icier regions of Europa's surface are relatively bright and light scattering. Light scattering produced by radiation damage in an ice surface has also been correlated with the prior loss of hydrogen that could otherwise form radiation-darkened hydrocarbons (*Strazzulla and Johnson,* 1991; *Strazzulla,* 1998; *Moroz et al.,* 2004). Scattering in the visible is usually associated with multiple defects that aggregate, forming inclusions in the ice. The presence of radiation damage inclusions is manifest not only by the scattering in the visible but also by the presence of molecular oxygen inclusions in Europa's surface produced by the radiation (*Johnson and Quickenden,* 1997; *Johnson and Jesser,* 1997). In these inclusions, the penetrating radiation also produces ozone.

Any organic molecules that reach Europa's surface from endogenic or exogenic sources are also subject to chemical modification and eventual destruction by continuing surface irradiation. In samples containing long chain molecules, chain breaks and cross-linking can occur, changing the character of the organic. Discrete peaks in a molecular mass spectrum can be indicative of biological sources but these peaks can be dispersed by radiation processing. A key issue for future observations is how and where to search for recognizable organic biosignatures that have not been highly degraded by irradiation (see also the chapter by Hand et al.). One approach is to identify regions of relatively low radiation exposure, e.g., on the leading hemisphere and/or in topographically shielded locations.

5. SUMMARY AND CONCLUSIONS

We have shown above that energetic particle fluxes typically increase inward through the middle and inner jovian magnetosphere, with very high intensities at Europa' orbit. It is also found that a part of the ion energy spectrum is heavily depleted because of charge exchange collisions with Europa's neutral gas torus. Many of these energetic ions are lost from the system before they reach Europa or points radially inward from that orbit. We also show that there are specific regions on Europa, particularly on the leading hemisphere, where the bombarding flux of some energetic electrons is relatively small. This is because the ratio of the speed of these particles parallel to the magnetic field line to the speed at which they are carried azimuthally around the magnetosphere is very large.

The radiation environment near Europa varies in time but only to a limited extent. At MeV energies, data reveal less scatter in the stronger magnetic field of the planet, as expected. This suggests that some of the variability due to injections and other types of magnetospheric activity are less likely, than is the case at Saturn, to dominate the fluxes near Europa for many species and energies. In fact, one study of the ≥11-MeV electron channel on Galileo over the entire orbital mission found that the standard deviation from the average value was only a factor of 2–3. In medium energy ions, the total integrated variation in sparse sampling over about 4 yr found a factor of ~2 variation. Future studies of the radiation environment and Europa's place in it would benefit from a more comprehensive measurement of the electron environment. Galileo made many close passes by the moon, but EPD was somewhat limited in its MeV electron coverage and we are learning these are important particles for reactions deep in the ice layer.

Regarding bombardment of Europa, we have argued that almost all charged particles preferentially impact Europa's trailing hemisphere, except >25-MeV electrons, which preferentially impact the leading hemisphere. For each species and energy, the interesting question is how the flux into the surface falls off between the trailing hemisphere apex and the leading one. Previous modeling has shown that 30- and 140-keV sulfur ions can bombard the entire surface by virtue of their gyro, bounce, and drift motions, and there are only small hemispherical differences. On the other hand, 1-keV sulfur ions have strong leading/trailing asymmetries. Energetic electrons between about 100 keV and 25 MeV preferentially bombard the trailing hemisphere. But 20-keV electrons can easily reach the poles at high flux levels. No particle tracing has been done that accounts for Europa's location in the current sheet or accounts for electromagnetic fields that self-consistently include contributions from the ionosphere and/or induced magnetic fields to further substantiate these claims.

In understanding the surface interactions, we have discussed dose vs. depth, radiolysis, sputtering, and radiation damage. We have attempted to link particle species and energies to various processes. For dose rates into the surface, we have emphasized the complexity in understanding the particles that dominate the energy into the layer by surface longitude and latitude and depth. For example, we do not expect many 100-keV electrons to reach Europa's poles, based on a simple picture of electron motion, but electrons of lower energies do reach the poles and contribute to the dose. Once this map of energy into the surface by species at each depth is known, surface properties themselves must be considered. For example, it would be interesting to compare bombardment maps with surface maps of reflectance spectra in a number of different spectral regions having very different sampling depths. We have also described how sputtering depends on ice porosity and temperature and that the sputtered products can escape, stick, etc. We also described how new molecules are formed in ice, how some easily escape and others are trapped. We raised the issue of the net flux of minor species out of a surface as an indicator of surface constituents. Finally, we considered the issue of survivability of species in ice due to radiation damage.

Acknowledgments. We appreciate assistance on this chapter from R. W. Carlson and B. Mauk, and conversations with T. Cassidy, R. B. Decker, D. Haggerty, I. Jun, S. Ohtani, W. Patterson, W. Paterson, and L. Prockter. The portion of this work provided by H.B.G. was carried out at the Jet Propulsion Laboratory, California Institute of Technology, under a contract with the National Aeronautics and Space Administration. J.F.C. acknowledges previous support from the NASA Jovian System Data Analysis Program for Galileo Orbiter data analysis and ongoing support from the NASA Planetary Atmospheres program for Europa surface and atmospheric environment modeling. R.E.J. acknowledges support by NASA Planetary Atmospheres and Planetary Geology Programs. C.P. would like to acknowledge NASA Planetary Atmospheres and Outer Planets Research grant support to JHU/APL.

REFERENCES

Burger M. H. and Johnson R. E. (2004) Europa's cloud: Morphology and comparison to Io. *Icarus, 171,* 557–560.

Carlson R. W., Anderson M. S., Johnson R. E., Schulman M. B., and Yavrouian A. H. (2002) Sulfuric acid production on Europa: The radiolysis of sulfur in water ice. *Icarus, 157,* 456–463.

Carlson R. W., Anderson M. S., Mehlman R., and Johnson R. E. (2005) Distribution of hydrate on Europa: Further evidence for sulfuric acid hydrate. *Icarus, 177,* 461–471.

Carlson R. W., Johnson R. E., and Anderson M. S. (1999) Sulfuric acid on Europa and the radiolytic sulfur cycle. *Science, 286,* 97–99.

Cassidy T. A. and Johnson R. E. (2005) Monte Carlo model of sputtering and other ejection processes within a regolith. *Icarus, 176,* 499–507.

Cassidy T. A., Johnson R. E., McGrath M. A., Wong M. C., and Cooper J. F. (2007) The spatial morphology of Europa's near-surface O_2 atmosphere. *Icarus, 191(2),* 755–764.

Chyba C. F. and Hand K. P. (2001) Life without photosynthesis. *Science, 292,* 2026–2027.

Chyba C. F. and Phillips C. B. (2001) Possible ecosystems and the search for life on Europa. *Proc. Natl. Acad. Sci., 98,* 801–804.

Cohen C. M. S., Stone E. C., and Selesnick R. S. (2001) Energetic ion observations in the middle jovian magnetosphere. *J. Geophys. Res., 106,* 29871–29882.

Connerney J. E., Acuna M. H., Ness N. F., and Satoh T. (1998) New models of Jupiter's magnetic field constrained by the Io flux tube footprint. *J. Geophys. Res., 103,* 11929–11940.

Cooper J. F. and Sturner S. J. (2007) Hemispheric and topographic asymmetry of magnetospheric particle irradiation for icy moon surfaces (abstract). In *Workshop on Ices, Oceans, and Fire: Satellites of the Outer Solar System,* p. 32. LPI Contribution No. 1357, Lunar and Planetary Institute, Houston.

Cooper J. F., Johnson R. E., Mauk B. H., Garrett H. B., and Gehrels N. (2001) Energetic ion and electron irradiation of the icy Galilean satellites. *Icarus, 149,* 133–159.

Cooper J. F., and Sturner S. J. (2006) Europa surface radiation environment for lander assessment (abstract). Paper presented at the Astrobiology Science Conference (AbSciCon) March 26–30, 2006, Washington, DC.

Divine N. and Garrett H. B. (1983) Charged particle distributions in Jupiter's magnetosphere. *J. Geophys. Res., 88,* 6889–6903.

Fillius W. (1988) Toward a comprehensive theory for the sweeping of trapped radiation by inert orbiting matter. *J. Geophys. Res., 93(A12),* 14284–14294.

Garrett H. B., Jun I., Ratliff J. M., Evans R. W., Clough G. A., and McEntire R. W. (2002) Galileo interim radiation model. *Jet Propulsion Laboratory Report D-24811,* Jet Propulsion Laboratory, Pasadena.

Garrett H. B., Levin S. M., Bolton S. J., Evans R. W., and Bhattacharya B. (2005) A revised model of Jupiter's inner electron belts: Updating the Divine radiation model. *Geophys. Res. Lett., 32,* DOI: 10.1029/2004GL021986.

Geissler P. E., Greenberg R., Hoppa G., McEwen A., Tufts R., et al. (1998) Evolution of lineaments on Europa: Clues from Galileo multispectral imaging observations. *Icarus, 135,* 107–126.

Grundy W., Buratti B. J., Cheng A. F., Emery J. P., Lunsford A., et al. (2007) New Horizons mapping and Ganymede. *Science, 318,* 234–237.

Gudipati M. S., Allamandola L. J., Cooper J. F., Sturner S. J., and Johnson R. E. (2007) Consequence of electron mobility in icy grains on solar system objects (abstract). *Eos Trans. AGU, 88(52),* Fall Meeting Supplement, Abstract P53B–1248.

Hand K. P., Chyba C. F., Carlson R. W., and Cooper J. F. (2006) Clathrate hydrates of oxidants in the ice shell of Europa. *Astrobiology, 6(3),* 463–482.

Hansen G. B. and McCord T. B. (2004) Amorphous and crystalline ice on the Galilean satellites: A balance between thermal and radiolytic processes. *J. Geophys. Res., 109,* E01012, DOI: 10.1029/2003JE002149.

Johnson R. E. (1990) *Energetic Charged Particle Interaction with Atmospheres and Surfaces.* Springer-Verlag, New York.

Johnson R. E. (1995) Sputtering of ices in the outer solar system. *Rev. Mod. Phys., 68,* 305–312.

Johnson R. E. (1998) Sputtering and desorption from icy surfaces. In *Solar System Ices* (B. Schmitt et al., eds.), pp. 303–331. Astrophys. Space Sci. Library Vol. 227, Kluwer, Dordrecht.

Johnson R. E. (2000) Sodium at Europa. *Icarus, 143,* 429–433.

Johnson R. E. and Jesser W. A. (1997) O_2/O_3 microatmospheres in the surface of Ganymede. *Astrophys. J. Lett., 480,* L79–L82.

Johnson R. E. and Quickenden T. I. (1997) Photolysis and radiolysis of water ice on outer solar system bodies. *J. Geophys. Res., 102,* 10985–10996.

Johnson R. E., Quickenden T. I., Cooper P. D., McKinley A. J., and Freedman C. G. (2003) The production of oxidants in Europa's surface. *Astrobiology, 3,* 823–850.

Johnson R. E., Carlson R. W., Cooper J. F., Paranicas C., Moore M. H., and Wong M. C. (2004) Radiation effects on the surfaces of the Galilean satellites. In *Jupiter: The Planet, Satellites and Magnetosphere* (F. Bagenal et al., eds.), pp. 485–512. Cambridge Univ., Cambridge.

Johnson R. E., Fama M., Liu M., Baragiola R. A., Sittler E. C. Jr., and Smith H. T. (2008) Sputtering of ice grains and icy satellites in Saturn's inner magnetosphere. *Planet. Space Sci., 56,* DOI: 10.1016/j.pss.2008.04.003.

Jun I., Garrett H. B., Swimm R., Evans R. W., and Clough G. (2005) Statistics of the variations of the high-energy electron population between 7 and 28 jovian radii as measured by the Galileo spacecraft. *Icarus, 178,* 386–394.

Kahin K., Combi M. R., Gombosi T. I., Nagy A. F., DeZeeuw D. L., and Powell K. G. (1999) On Europa's magnetospheric interaction: A MHD simulation of the E4 flyby. *J. Geophys. Res., 104,* 19983–19992.

Khurana K. K. and Kivelson M. G. (1993) Inference of the angular velocity of plasma in the jovian magnetosphere from the sweepback of magnetic field. *J. Geophys. Res., 98,* 67–79.

Kivelson M. G., Khurana K. K., Stevenson D. J., Bennett L., Joy S., Russell C. T., Walker R. J., Zimmer C., and Polanskey C. (1999) Europa and Callisto: Induced or intrinsic fields in a periodically varying plasma environment. *J. Geophys. Res., 104,* 4609–4625.

Lagg A., Krupp N., and Woch J. (2003) In-situ observations of a neutral gas torus at Europa. *Geophys. Res. Lett., 30,* DOI: 10.1029/2003GL017214.

Leblanc F., Johnson R. E., and Brown M. E. (2002) Europa's sodium atmosphere: An ocean source? *Icarus, 159,* 132–144.

Lindsay B. G. and Stebbings R. F. (2005) Charge transfer cross sections for energetic neutral atom data analysis. *J. Geophys. Res., 110,* A12213, DOI: 10.1029/2005JA011298.

Mauk B. H., Williams D. J., McEntire R. W., Khurana K. K., and Roederer J. G. (1999) Storm-like dynamics of Jupiter's inner and middle magnetosphere. *J. Geophys. Res., 104,* 22759–22778.

Mauk B. H., Mitchell D. G., Krimigis S. M., Roelof E. C., and Paranicas C. P. (2003) Energetic neutral atoms from a trans-Europa gas torus at Jupiter. *Nature, 421,* 920–922.

Mauk B. H., Mitchell D. G., McEntire R. W., Paranicas C. P., Roelof E. C., Williams D. J., and Lagg A. (2004) Energetic ion characteristics and neutral gas interactions in Jupiter's magnetosphere. *J. Geophys. Res., 109,* DOI: 10.1029/2003JA010270.

McCord T. B., Hansen G. B., Fanale F. P., Carlson R. W., Matson D. L., et al. (1998) Salts on Europa's surface detected by Galileo's Near Infrared Mapping Spectrometer. *Science, 280,* 1242–1245.

McCord T. B., Hansen G. B., Matson D. L., Johnson T. V., Crowley J. K., et al. (1999) Hydrated salt minerals on Europa's surface from the Galileo near-infrared mapping spectrometer (NIMS) investigation. *J. Geophys. Res., 104,* 11827–11852.

Moroz L. V., Baratta G., Strazzulla G., Starukhina L., Dotto E., Barucci M. A., Arnold G., and Distefano E. (2004) Optical alternation of complex organics induced by ion irradiation: 1. Laboratory experiments suggest unusual space weathering trend. *Icarus, 170,* 214–228.

Paranicas C., McEntire R. W., Cheng A. F., Lagg A., and Williams D. J. (2000) Energetic charged particles near Europa. *J. Geophys. Res., 105,* 16005–16015.

Paranicas C., Carlson R. W., and Johnson R. E. (2001) Electron bombardment of Europa. *Geophys. Res. Lett., 28,* 673–676.

Paranicas C., Ratliff J. M., Mauk B. H., Cohen C., and Johnson R. E. (2002) The ion environment of Europa and its role in surface energetics. *Geophys. Res. Lett., 29,* DOI: 10.1029/2001GL014127.

Paranicas C., Mauk B. H., Khurana K., Jun I., Garrett H., Krupp N., and Roussos E. (2007) Europa's near-surface radiation environment. *Geophys. Res. Lett., 34,* L15103, DOI: 10.1029/2007GL030834.

Paterson W. R., Frank L. A., and Ackerson K. L. (1999) Galileo plasma moments at Europa: Ion energy spectra and moments. *J. Geophys. Res., 104,* 22779–22791.

Pospieszalska M. K. and Johnson R. E. (1989) Magnetospheric ion bombardment profiles of satellites: Europa and Dione. *Icarus, 78,* 1–13.

Shi J., Teolis B. D., and Baragiola R. A. (2007) Irradiation enhanced adsorption and trapping of O_2 on microporous water ice. *AAS/Division for Planetary Sciences Meeting Abstracts, 39,* 38.04.

Smyth W. H. and Marconi M. L. (2006) Europa's atmosphere, gas tori, and magnetospheric implications. *Icarus, 181,* 510–526.

Spencer J. R. and Calvin W. M. (2002) Condensed O_2 on Europa and Callisto. *Astron. J., 124,* 3400–3403.

Strazzulla G. (1998) Chemistry of ice induced by bombardment with energetic charged particles. In *Solar System Ices* (B. Schmitt et al., eds.), pp. 281–301. Astrophys. Space Sci. Library Vol. 227, Kluwer, Dordrecht.

Strazzulla G. and Johnson R. E. (1991) Irradiation effects on comets and cometary debris. In *Comets in the Post Halley Era, Volume 1* (R. L. Newburn Jr. et al., eds.), pp. 243–275. Kluwer, Dordrecht.

Sturner S. J., Shrader C. R., Weidenspointner G., Teegarden B. J., Attié D., et al. (2003) Monte Carlo simulations and generation of the SPI response. *Astron. Astrophys., 411,* L81–L84.

Thomsen M. F. and Van Allen J. A. (1980) Motion of trapped electrons and protons in Saturn's inner magnetosphere. *J. Geophys. Res., 85,* 5831–5834.

Walt M. (1994) *Introduction to Geomagnetically Trapped Radiation.* Cambridge Univ., Cambridge.

Zombeck M. V. (1982) *Handbook of Space Astronomy and Astrophysics.* Cambridge Univ., Cambridge.

Europa's Interaction with the Jovian Magnetosphere

Margaret G. Kivelson and Krishan K. Khurana
University of California, Los Angeles

Martin Volwerk
Österreichische Akademie der Wissenschaften

Europa is embedded in Jupiter's magnetosphere where a rapidly flowing plasma interacts electromagnetically with the moon's surface and its atmosphere. In this chapter, the phenomenology of the interacting system is presented and interpreted using both qualitative and quantitative arguments. Challenges in understanding the plasma environment arise partly because of the diverse scale-lengths that must be considered as well as the nonlinear nature of the interactions. The discussion that follows describes selected aspects of the interacting system. On the scale of gyroradii, we describe the effects of newly ionized particles on fields and flows and their relation to wave generation. On the scale of Europa radii, we discuss the structure of the local interaction. On the scale of the tens of Jupiter radii that separate Europa from Jupiter's ionosphere, we describe the aurora generated near the magnetic footprint of Europa in Jupiter's upper atmosphere. We end by stressing the relevance of plasma measurements to achievement of goals of a future Europa Orbiter mission.

1. INTRODUCTION

The Galilean moons, although small, play a distinctive role in the history of solar system science. Galileo recognized that their motions in periodic orbits around Jupiter were compelling analogs of planetary bodies in a heliocentric system (see chapter by Alexander et al.). The complex orbital interactions of the inner moons were found to account not only for orbital stability (e.g., *Goldreich,* 1965), but also for enhanced tidal heating (*Peale et al.,* 1979), which powers volcanic activity on Io and melting of the ice beneath the surface of Europa. That fluid oceans could be present beneath the icy crusts of the three outer moons was discussed (*Lewis,* 1971) decades before spacecraft observations provided support for (if not full confirmation of; see chapter by Khurana et al.) this speculation for some of the moons, in particular, Europa.

Concurrent with studies of the interior, the particle and fields environments of the moons began to attract attention following the discovery of Io's control of jovian decametric emissions (*Bigg,* 1964). *Goldreich and Lyndon-Bell* (1969) recognized that an electromagnetic link between the moon and Jupiter's ionosphere could explain the observations, a suggestion that implied the presence of plasma along the Io magnetic flux tube. Somewhat later, the existence of an extended nebula around Io's orbit, the Io torus, was established (*Kupo et al.,* 1976; *Mekler and Eviatar,* 1977). Io soon became the focus of *in situ* particle and field measurements by Voyager 1, and the ionian source of heavy ion plasma that shapes the structure of much of the magnetosphere was recognized (*Bagenal and Sullivan,* 1981; *Shemansky and Smith,* 1981; see also review by *Thomas et al.,* 2004). Europa, the smallest of the Galilean moons, was found also to be a plasma source (*Intriligator and Miller,* 1982; *Eviatar and Paranicas,* 2005; *Russell et al.,* 1999), albeit a secondary one. However, Europa's plasma environment received comparatively little attention until it was established by Galileo observations that its geologically young surface lies above what is probably a global ocean (*Khurana et al.,* 1998). This discovery promoted the priority of Europa and its local plasma environment as targets for further planetary exploration. Although only 3 of the 12 flybys of the Galileo prime mission (1995 through 1997) passed close to Europa, the next phase of the mission, designated the Galileo Europa mission, devoted half of its 14 flyby opportunities to Europa. Table 1 summarizes various relevant features of Galileo's flyby trajectories (or "passes") plotted in Fig. 1. The final stage of Galileo's odyssey included a specially designed pass in which magnetometer measurements found a predicted reversal of the orientation of the internal dipole moment, thus confirming the presence of an inductive field at Europa (*Kivelson et al.,* 2000).

This chapter addresses the subject of Europa's interaction with the particles and fields of the jovian magnetosphere. The topic presents a considerable challenge because the moon and its maguetized plasma environment interact nonlinearly. Relevant to the interaction are matters as diverse as the chemical composition of the surface from which particles are sputtered, the properties of the energetic particles responsible for the sputtering, the temporal and spatial characteristics of the magnetospheric plasma near the orbit of Europa, properties of the magnetic field that confines the plasma, and the electromagnetic characteristics of the moon and its ionosphere. Europa's response to

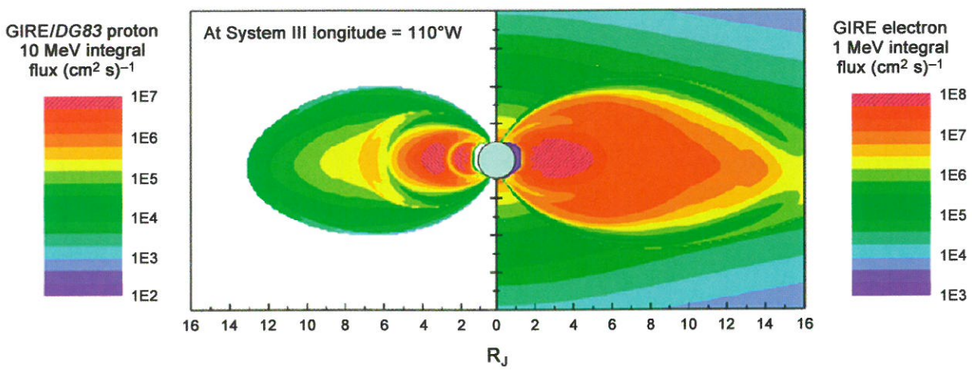

Plate 26. Contour plots of the GIRE/*DG83* model E > 10 MeV integral proton (left) and E > 1 MeV electron (right) fluxes for the vovian magnetosphere radiation region. The model provides the flux as a function of position, energy, and pitch angle. The fluxes presented here have been integrated over pitch angle. Note that outside the contour of L = 12, the proton model is set to 0, whereas the electron model fluxes outside L = 16 are only approximate since they are not considered trapped in the model (see *DG83* for details). Figure courtesy of I. Jun.

Accompanies chapter by Paranicas et al. (pp. 529–544).

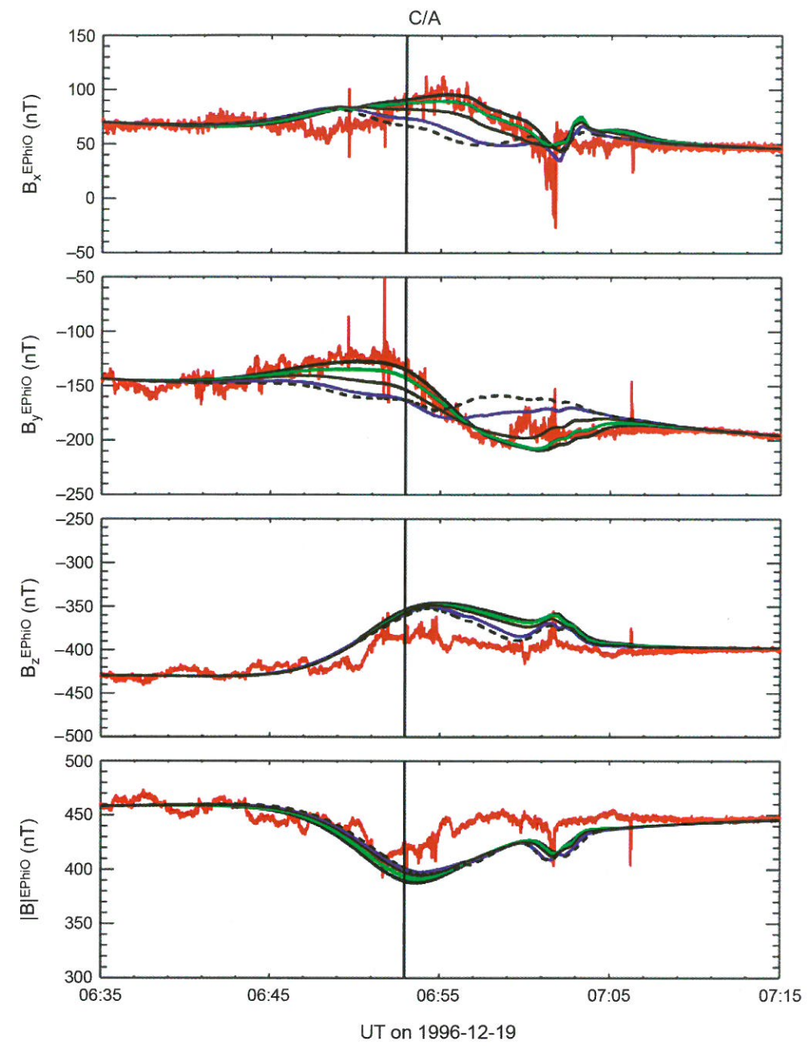

Plate 27. Observed and modeled magnetic field for the E4 flyby. Red = measurements of *Kivelson et al.* (1997); dashed black = modeled field with no internally induced field; Blue, green, and black = modeled field including induction in a 100-km-thick ocean lying beneath a crust of 25 km for ocean conductivities of 100, 250, and 500 mS/m, respectively. From *Schilling et al.* (2007).

Accompanies chapter by Kivelson et al. (pp. 545–570).